Integrated Optics for Holographic Video

by

Daniel E. Smalley

Submitted to the Department of Electrical Engineering and Computer Science
in partial fulfillment of the requirements for the degree of

Master of Engineering in Electrical Engineering and Computer Science

at the

MASSACHUSETTS INSTITUTE OF TECHNOLOGY

September 2006

Author .....
Department of Electrical Engineering and Computer Science
August 18, 2006

Certified by .....
V. Michael Bove
Principal Research Scientist
Thesis Supervisor

Accepted by .....
Arthur C. Smith
Chairman, Department Committee on Graduate Students

Integrated Optics for Holographic Video

by

Daniel E. Smalley

Submitted to the Department of Electrical Engineering and Computer Science
on August 18, 2006, in partial fulfillment of the
requirements for the degree of
Master of Engineering in Electrical Engineering and Computer Science

Abstract

The goal of this research is to fabricate a guided-wave, two-axis scanner and to modify the design of the MIT holovideo system to take full advantage of the scanner's high bandwidth and two-dimensional deflection. The new display geometry will be designed to use the guided-wave scanner coupled with a holographic optical element to perform a solid-state horizontal de-scan. The development of the guided-wave scanner and the improvements made to the holovideo geometry, will enable the construction of a third generation holovideo display that is higher bandwidth, more solid-state and at least an order of magnitude less expensive than previous generations.

Thesis Supervisor: V. Michael Bove
Title: Principal Research Scientist

Acknowledgments

I would like to give my sincere thanks to three people who believed in my work even when they had little reason to do so:

My wife, Pamela, who has been cheerfully enduring years of penury while I pursue my mad-scientist ambitions.

Elroy Pearson, who plucked me out from among the turkey farms of rural Utah and gave me the opportunity to work as an intern at the Media Lab. The earliest sparks of this work were struck during our lunchtime conversions about how to make holovideo out of Aluminum foil and plastic forks.

Dr. Bove, who has coached this work both formally and informally from the very beginning, bestowing countless gems of wisdom and making a sincere effort to keep me from accidentally microwaving my liver or searing my eyeballs.

I would also like to thank: Quinn Smithwick, for his collaboration and dedication to "making [my holovideo] dreams come true." Diane Hirsh, Jeevan Kalanithi and Jim Barabas for putting up with prolonged holovideo discussions during group meetings. All the folks at NSL, MTL and SEBL, who gave me access to their facilities and valuable fabrication advice. Neil Gershenfeld, Scott Manalis and their respective graduate students for allowing me to use their wirebonder and RF test equipment.

Contents

List of Figures

List of Tables

Chapter 1

Introduction

1.1 Improving MIT's Holovideo System

This thesis describes the development of a guided-wave scanner for the third generation MIT holographic video system, called Mark III. The integrated two-dimensional scanner will be used in Mark III to increase the total system bandwidth, to reduce noise and to eliminate the need for fast horizontal de-scanning mirrors. Through the improvements, made possible by the introduction of the guided-wave scanner, we seek to arrive at a display that is approximately the size and cost of a common CRT monitor.

1.2 Why Holographic Video?

1.2.1 The Ideal Holographic Display

In terms of realism, holographic video is potentially superior to all other 3D display techniques—whether they be stereoscopic, view-sequential or volumetric. Every non-holographic display is missing at least one of the visual cues that are important for depth perception. By contrast, holographic images can be made to possess all the depth cues of an actual object, including those of accommodation (focus) and occlusion, by faithfully reconstructing optical wavefronts. The light pattern radiating from

a hologram of an object may be made identical to the light pattern emanating from the object itself.[1] In addition to giving holographic images convincing depth, optical wavefront reconstruction also allows holograms to exhibit angle-dependent lighting effects like specular reflection, refraction and iridescence. Optically, the output of a holographic display can be treated as a real object: it may be examined with a microscope, imaged with lenses, or even *holographed*. We might go so far as to argue that an ideal holographic display is in fact the 'universal display,' because it could be made to emulate the output of any other direct-view, three-dimensional display.

1.2.2 Divergence from the Ideal Display

The display described in this work is not 'ideal' in that it will be a *horizontal parallax only* (HPO) display and as a result suffer from astigmatism, but the claims made for the ideal system will still be valid for horizontal information which is more important than vertical information for three-dimensional perception in humans. The flexibility of integrated optics, may be a key enabler for adding full parallax in the future implementations of the MIT architecture and for helping the MIT system more closely approach the ideal holographic display described above.

1.2.3 Holographic Display Applications

A large, inexpensive, HPO, three-dimensional display would have application in art, education, scientific imaging and medical visualization. Applications would include the visualization of complex three-dimensional datasets ranging from gene sequencing information to seismic data for oil well searches. A high performance display could be useful in representing complicated three-dimensional structures like photonic crystal lattices or complex molecular models. In medicine, a high quality three-dimensional model made from MRI information might be used to enhance surgical planning. In the future, a holographic display coupled with haptic interaction technology [15] could

[1] This equivalence of optical wavefronts is the principle upon which interferometry relies. Diffraction can produce optical wavefronts equivalent to those produced by real objects, given that they are illuminated with monochromatic illumination.

enable remote treatment, or 'telemedicine', through which a doctor in Germany aided by force feedback tools and a holographic display, could remotely perform surgery on a patient in Australia. However, in order for holovideo to be used in any of these applications, we must first overcome some of the fundamental limitations found in the designs of the previous holovideo prototypes.

1.2.4 Goals for Mark III

The first two scanned-AOM holovideo prototypes, named Mark I and Mark II, were robust and effective systems that established themselves as the "first practical holographic video display[s]"[22] but they were not built in a form intended for commercialization. They each filled large optics table with expensive custom modulators, lenses and either a fast scanning mirror or an even faster spinning polygon. Pierre St. Hillaire, who constructed the second generation display, predicted that the Mark II might be to holovideo what the mechanical Nipkow disk was to modern television [22], that is, the mechanical predecessor of a more elegant solid-state solution. We hope to meet the challenge articulated by Dr. Bove, the current holovideo principal investigator, to create a holographic video display of approximately "the size and cost of a CRT monitor." Incremental improvements to the previous generation technology will not be enough, what we need now is not a better "Nipkow disk," but rather, the holovideo equivalent of the cathode ray tube.

The cathode ray tube analogy for holographic video is the *guided-wave scanner* (GWS) paired with special de-scanning *holographic optical elements* (HOEs). By using the GWS with de-scannig HOEs we can overcome the limitations of previous generations of the MIT holovideo system. Each component of the physical geometry of the Mark III has been constructed around the GWS/HOE system using materials and processes that are suitable for mass-production. The guided-wave modulator may be batch-fabricated using planar, photolithographic processes and the reduced requirements on the supporting optics will allow the final display to be made primarily from stock optics using standard tools and techniques.

Bandwidth

The most fundamental advancement in the Mark III design is its increased bandwidth per channel. When Dr. Stephen Benton was asked what he thought an improved holovideo light modulator needed, he said only one word, "Bandwidth!" One channel of the GWS provides more bandwidth than all the eighteen channels found in the Mark II's *Acousto-Optic Modulator* (AOM). Achieving high bandwidth in a holographic video system makes it possible to have a wider viewing angle, a larger image size and a higher refresh rate; it is also key to the inclusion of full-color and full-parallax. The relationship between bandwidth and system parameters is given by Quinn Smithwick to be:

$$\Delta F \propto \frac{W\theta * lpf * fps}{\lambda} \tag{1.1}$$

With increased RF bandwidth, ΔF, we can either increase the display width, W, the view angle, θ, the lines per frame, lpf, the frames per second, fps, or decrease the illumination wavelength, λ.

If we multiply the bandwidth by the aperture of the modulator, d, and divide by the velocity of sound in the crystal, v, we get the total number, N, of light spots resolvable by the scanner which corresponds rougly to the maximum, diffraction-limited, number of views available to the display.[2] In the Mark III system, the bandwidth is 1Ghz, the aperture 3mm and the velocity 3909m/s giving us:

$$N = \frac{\Delta F d}{v} = 767 views \tag{1.2}$$

Solid-State De-Scan

The holographic pattern in the guided-wave scanner is collection of sound waves that travels at 3909m/s. In order for the pattern to appear stationary, it is necessary to op-

[2]The actual number of views can be chosen to be less than this upper limit. The holographic patterns generated for Mark II currently use approximately 200 views. Talking about a maximum number of diffraction limited views is just one way of thinking about the diffractive numerical aperture of the system which is what N really represents.

tically de-scan the image of the moving acoustic fringes. De-scanning was performed by a rotating polygonal mirror in Mark I and by a bank of galvonometers in Mark II. In Mark III, a static helical mirror is used to de-scan the holographic pattern. The process which creates the HOE encodes the temporal function of a horizontal scanning mirror as a spatial function on the HOE. The resulting horizontal deflection of a beam scanning vertically on the HOE is the same as horizontal deflection that would result from reflecting light off of a horizontal scanning mirror.

System Cost

The GWS itself is an integrated optical device that is readily batch fabricated with only two photolithographic steps, and could be made inexpensively in large quantities. HOEs may also be reproduced inexpensively once a suitable master is made. The cost of lenses and the vertical scanner would probably not be reduced as significantly as the scanner and the HOEs by mass-production, but there is a good possibility that some of the geometric optics will be brought on-chip and made part of the integrated-optics portion of the display.

1.2.5 Design Criteria for the GWS

Ultimately, the objective of this work is to apply all the solutions mentioned earlier to the creation of a working display, but first, each of these technologies must be developed to meet their respective design criteria. In particular, the GWS device should be able to couple, confine, diffract and mode convert laser light. It should be able to diffract light horizontally over a gigahertz frequency range and mode-couple light over a 50MHz bandwidth.

1.3 Integrated Optics to Improve Holovideo

The Mark III display is a significant, not-merely incremental, improvement on earlier generations. The technology that now sits at the heart of the display, the Guided Wave Scanner, is drawn from fields quite apart from the bulk optical modulators that

made up earlier versions of the display. The guided-wave nature enables an acousto-optic interaction that is more efficient than the interaction in bulk modulators. There is also more design flexibility for a surface wave device than for a bulk modulator. Additionally, as a SAW device, future improvements of the modulator's design may be taken from the past three decades of mature surface acoustic wave research as well as from the current innovation in the field of integrated optics.

The GWS provides the first economic solution for electroholography and a more feasible platform for the new medium of holographic video. We can expect that these improvements will help establish holovideo as a ubiquitous tool for professionals and laymen alike.

Although the holovideo system is nominally a display, because of its unique light modulation technique and de-scan strategy, it may find its most promising applications as part of more sophisticated optical systems in adaptive optics or in interferometry. Alternately, trivial modifications to the core display may result in the development of a hardcopy holographic printer, a personal projection device or other novel devices that involve the unbroached application of integrated acousto-optics for macro-scale laser modulation and projection display.

1.4 Evaluating Integrated Optics as a Solution

Guided-wave optical devices were identified as the most promising solution for the task of light modulation in holovideo only after first considering several other options which included: Lithium Niobate bulk Bragg modulators, LCD and MEMs structures [14] and reflective-mode surface acoustic wave modulators (SAWmods).

1.4.1 Lithium Niobate Bragg Cell Modulators

Lithium Niobate Bragg-cell modulators have been constructed to have bandwidths in excess of 2.5GHz, which in Lithium Niobate translates to approximately 24 degrees of angular diffraction [16]. Unfortunately, even with advanced fabrication techniques, these devices lack the design flexibility that is found in planar devices and could

never be made as inexpensively as those fabricated from standard photolithographic, wafer-based processes.

1.4.2 MEMs Mirrors and LCD Modulators

Integrated devices like MEMs mirrors and LCD modulators currently possess moderate bandwidths but are prevented from achieving resolutions suitable for holographic video by their supporting circuitry. As photolithography improves, LCDs may eventually be of sufficiently high resolution to be by themselves full-parallax, diffractive light modulators. However, even when they achieve this resolution, it is unlikely that they will be produced as inexpensively as a guided-wave device which can already provide the requisite resolution for holographic video applications.

1.4.3 Surface Acoustic Wave Modulators

Surface acoustic wave modulators (SAWmods) [7]—which are essentially the reflection-mode dual of the GWS—were pursued and then abandoned. They have a very small interaction length which leads to poor diffraction efficiency (1%) spread over multiple orders. By comparison, the GWS uses Bragg diffraction which creates one order with an efficiency that may approach 100%.

1.4.4 The Guided-Wave Scanner

The GWS device is at once both a simple and subtle device which, as was mentioned earlier, provides an elegant solution for most of the problems associated with holographic video. It consists merely of a slab of Lithium Niobate, $LiNbO_3$, that is immersed in a melt of weak acid, and then used as a substrate for the patterning of Aluminum transducers. Yet, despite the simplicity of its construction, it is able to scan both horizontally and vertically as well as rotate the polarization of the modulated light making it possible to extract any unidiffracted noise with polarizers. The weak acid bath porcess called *proton exchange* is less involved than most kitchen recipes. The subsequent fabrication is largely completed by two photolithographic

steps, requiring only one high resolution mask, and two deposition steps. In contrast to most CMOS processes, which typically require 10-12 masks, this fabrication routine is extremely simple. It is nearly identical to that used for the fabrication of surface acoustic wave (SAW) filters. Much of the knowledge accumulated for SAW design can be brought to bear on the problem of creating high efficiency, high performance guided-wave acousto-optic modulators. Guided wave devices may eventually be made as inexpensively as SAW filters which cost a few dollars each to fabricate in large quantities (i.e. currently, a SAW filter centered at 940MHz can be bought from Digikey for $3.57).

1.4.5 Arriving at the HOE Solution.

The HOE solution was also arrived at, only after considering several alternative incarnations for static horizontal de-scan including prisms and helical mirrors. The key advantage of the HOE over a mirror or refractive optic is that it can be made to have a continuous horizontal modulation without modulating the light appreciably in the vertical axis. With refractive or reflective optics the surface normals caused vertical distortion that is fundamentally coupled to the horizontal de-scan. In fact, in order to get around this coupling to create the HOE, it was necessary to use a helical mirror, created by project collaborator, Quinn Smithwick, and then optically extract its vertical information using a Fourier-Plane spatial filter before the output light reached the recording surface. The HOE master does not have to be recorded optically. We understand the analytic structure of the diffraction pattern and should be able to directly write the master with an ebeam writing system capable of writing analog patterns of the appropriate resolution. For the moment, optical techniques are more practical. The HOE is also the least expensive option, among its competitors, for mass-manufacture.

1.4.6 Summary

In summary, a combination of the GWS (for light modulation) and the HOE (for de-scan along with a Dr. Smithwick's overhauled supporting geometry) forms a display that is singularly flexible, powerful, inexpensive and, in some cases, more nearly solid state than the other modulation solutions considered above. Additionally, there is the added bonus of polarization rotation of diffracted light that allows noise to be extracted with polarizers. These advantages, taken together, point to the GWS/HOEs approach as being particularly well suited for the next generation holographic display.

1.5 Overview of this Thesis

This thesis gives an overview of three-dimensional display technologies, gradually focusing on the Mark III in the context of other holovideo displays including its own progenitors. It also reviews the key theory related to the GWS's function as well as a more detailed description of the HOEs fabrication. The design, fabrication and analysis of the GWS are reported in detail. The thesis concludes with a summary of the GWS scanners performance to date and suggestions are given for future work.

Chapter 2

Three-Dimensional Display Technologies

People have been making three-dimensional displays since the Victorian era, so it should come as no surprise that today there are scores of three-dimensional display technologies. Almost all of these displays can be separated into three general categories: discretized view zone, volumetric and holographic displays. One category of displays is distinguished from the next by the three-dimensional depth cues it provides to the viewer as summarize in Table 2.1. The cues that have been demonstrated to be important[13] to three-dimensional perception are stereoscopy, motion parallax, accommodation and occlusion. This table is an over-generalization, but it is useful for understanding the advantages and limitations of the dozens of different three-dimensional displays available.

Display Type	Stereoscopy	Parallax	Accommodation	Occlusion
Discretized View Zone	•	•		•
Volumetric	•	•	•	
Holographic	•	•	•	•

Table 2.1: Three-dimensional displays and their respective depth cues.

2.1 Discretized View Zone

Discretized view zone describes a large family of displays which present a set of two-dimensional images that vary discretely with space and/or angle. The simplest implementation of this class of display is the stereoscope which provides one pair of two-dimensional views with one image per view—one image for the left eye and one image for the right eye. We can improve this display by increasing the number of views, allowing the viewer to move his/her eyes from one set of disparate views to another in order to give the viewer "motion parallax." This type of display is limited in two important ways: the viewer is relegated to an optimal viewing position and the viewer cannot look at the output of the display for long without suffering eye fatigue because stereopsis is not being reinforced by other depth cues.

2.1.1 The View Zone

It should be clear that for this type of display to work you have to make some assumptions about where the viewer's eyes are located. For a display with angularly discretized views, one eye may see more than one view at a time if the viewer is closer than expected. If the viewer if farther away than expected, one eye may see no view at all. For a view-sequential display, this set of scenarios may occur in reverse with overlapping views at a distance. This leads to the assumption of a 'viewing zone' or 'sweet spot' region which typically takes the form of a slotted or checkered window in space. If you are standing at the plane of the view zone, images at the display look three dimensional, but if you move outside of the view zone the 3D effect breaks down. Until recently, all free-view stereographic displays: lenticular, barrier-line and auto-stereo displays had this fundamental view zone limitation. However, recently head-tracking or eye-tracking systems have been used to adjust the view zone in real-time. When these systems become fluid enough to be convincing, they may effectively free the viewer from being confined to a view zone.

2.1.2 Stereopsis

Stereoscopic disparity and motion parallax are strong visual cues for the perception for three-dimensionality, but they are insufficient by themselves to prevent eyestrain. This is because stereographic displays are incapable of providing monocular accommodation. Each view in a stereographic display typically originates from a display screen. The viewer's eyes, working together, try to converge on the virtual point in space suggested by the intersection of the disparate 2D views, but each eye individually focuses (accommodates) on the display screen. Since the eye is not converging and focusing at the same point, it becomes strained.[2]

Still stereographic displays are relatively easy to build and can have a low bandwidth requirement. Lenticular and barrier-line displays are finding their way into cell phones and laptops and it is hoped that widespread use of these displays will prepare consumers for more sophisticated three-dimensional offerings as they become available.

2.2 Volumetric Displays

Volumetric displays include: swept-volume displays, space-sequential displays, laser direct-write displays that create luminescence in polymers or in air using plasma discharge, fireworks displays, jars filled with fireflies etc.

In a volumetric display, every point that an observer sees originates from a *luminous* or *illuminated* bit of matter—the surface of a spinning disk, a light emitting diode or a speck of glowing plasma. Since every image point originates from a tangible object, the viewer experiences no eyestrain. However, the key limitation of volumetric displays is that they produce image points which are transparent to one another so that one luminous object cannot fully occlude another. Therefore all the displayed

[2]This is not true in the limit of many views. If, for example, the views are so densely packed that two views enter the pupil simultaneously, the eye can be made to accommodate on the virtual point. In this limit, discrete-view displays become continuous and begin to exhibit some of the characteristics of holographic displays—though the superposition of views does not, in general, add coherently as is the case for holographic wavefronts.

images are either surface hulls or translucent 'ghosts.'[3] This inability to occlude light stems from the fact that volumetric points of light look fundamentally the same from every angle. In discretized-view displays or in holographic displays, a point can be made to appear bright at one angle and then be immediately extinguished in the next, only to reappear a different color in the next. This control of angular view is essential for occlusion and also for the display of many light phenomena (caustics) including refraction, specular reflection, scattering and iridescence (interference). The lack of occlusion or caustics may not be a detriment for many applications that value abstraction over realism. For example, in air traffic control you primarily concerned with knowing the real-time *location* of aircraft. It really does not matter whether the images look like glistening, photorealistic aircraft or like glowing blips as long as you can accurately gauge their relative 3D positions. If, however, you seek to produce images with a high degree of realism, you will need the increased image control that a holographic display provides.

2.3 Holographic Displays

Holographic displays use diffraction to form images that possess all four depth cues, and have the potential to display images that appear nearly indistinguishable from their material counterparts. You can already observe this level of realism in static full color reflection holograms and pulsed laser portraits. As holographic displays improve, they too, may approach this level of realism and may, by adding the temporal dimension, surpass all that has been previously achieved. It may be that in the near future, when we glance out our windows, we will not be entirely sure we are not actually looking into a holographic video display.

So if holographic displays are so great, why isn't everyone making them? The answer to this question is that while holovideo displays can be conceptually simple

[3]Notably, volumetric displays are solving the Princess Leia "hologram" problem which requires nearby air to be either a light modulator or a light source. Different volumetric displays have been able to manipulate air to function in both of these ways; unfortunately these methods involve high-powered laser beams, plasmas, weapons-grade sonic transducers or other human-unfriendly items.

they pose a practical challenge. The image control that is available to a holographic system is enormous, but so is the information required to run the display. Consider the fact that two, twenty or two hundred people observing the display from different angles may be made to see entirely different scenes or perhaps the same scene predistorted to compensate for the observer's respective eyeglass prescription. All of this information has to be encoded somewhere, and that somewhere is in a *diffraction pattern*. A diffraction pattern is just a collection of lines, called *fringes*, that is so dense that light diffracts significantly as it passes through the pattern. The more dense the pattern, the more extreme the angle of diffraction. You can encode (usually by amplitude or phase modulation) sparse lines with the information that you want to project at low angles, and dense lines with information that you want to project at high angles. The superposition of these line patterns becomes your diffraction pattern. Light passing through the diffraction pattern faithfully reconstruct the encoded angular information. A hologram, it turns out, is nothing more than a diffraction pattern, and a holographic display, in turn, is nothing more than a diffraction pattern that can be updated at video rates. A display-worthy hologram will diffract light over an angular range of 30 degrees or more, be wide enough for a viewer to stand at a short distance (0.5m), and have both eyes fit comfortably within the angular output of the hologram and have a little freedom to move from side to side. For this angle of diffraction, we can solve for the minimum pixel size by using the 'Bragg' or 'grating' equation.

$$\sin\theta_{out} - \sin\theta_{in} = \frac{m\lambda}{\Lambda} \tag{2.1}$$

To get 30 degrees of diffraction, assuming normal incident light or plus/minus 15 degrees of diffraction, we need to write pixels of approximately $\frac{\Lambda}{2}$,

$$\frac{m\lambda}{4 * \sin(15^\circ)} = 0.6\mu m$$

A pixel six-tenths of a micron in size corresponds to 41000dpi resolution, which is more that an order of magnitude higher in density than what today's high-end printers

can produce. How then are we going to write such fine patterns over the entire area of a display screen, let alone rewrite the whole frame at video rates? Instead of dozens of displays as we saw before, we find ourselves with only a handful of contenders, and currently only the scanned AOM displays are able to simultaneously meet the requirements of large viewing angle and video-rate update.

2.3.1 OASLM Holographic Displays

T.C. Poon Display, 1993

Dr. Poon has created several displays, which include an OASLM written with an ebeam[17]. This system is reminiscent of the Eudiphor projector which wrote a diffraction pattern with an ebeam on a layer of oil. Instead of oil, the Poon display writes on an Optically-Addressed Spatial Light Modulator (OASLM). An OASLM is an LCD panel that has a photosensitive layer instead of a backplane. It is unlikely, however, that the bandwidth of ebeam writing technology will improve to match that of tiled microdisplay or acousto-optic modulator schemes.

QinetiQ Display, 2004

QinetiQ has developed a display that tiles the output of a fast 1Ghz bandwidth Electrically Addressed Spatial Light Modulator (EASLM) onto an Optically Addressed Spatial Light Modulator (OASLM)[4]. A shutter in front of a wall of lenses allows the display to write de-magnified images of the EASLM onto abutting regions at the OASLM. This display boasts modular design, full-parallax and full color.

2.3.2 DMD Holographic Display, 2004

Bala Munjuluri and his colleagues at the University of Texas, use a Digital Mirror Device (DMD) as a dynamic holographic grating[11]. This means that the display has a relatively low bandwidth requirement and a low-cost, straight-forward design. However the low bandwidth means low diffraction angle, so the output of the display is projected into an omni directional diffuser that is meant to widen the angle of view,

but unfortunately also has the effect of turning this display's holographic points into volumetric points!

2.3.3 Scanned AOM Holographic Displays

The MIT Mark I, 1990

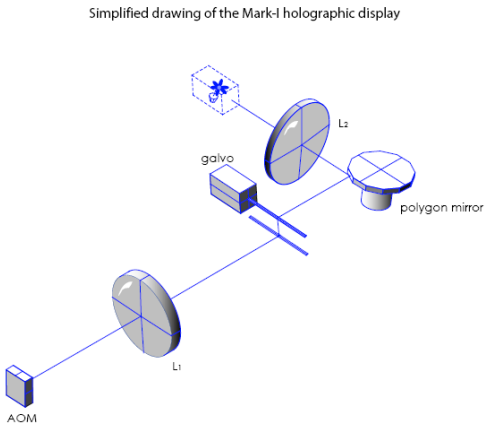

Figure 2-1: The Mark I Holovideo Display

MIT's Mark I[1] uses a Tellurium Dioxide (TeO_2) Acousto-Optic Modulator (AOM). Piezo transducers on one side of the AOM launch a pattern of sound waves that travel through the volume of the crystal. Laser light passing through the crystal is diffracted by the sound waves. The movement of the pattern in the crystal is corrected optically through the use of a rotating polygonal mirror that de-scans the wavepattern on the AOM. The horizontal 'hololine' that results is then scanned vertically with a galvo-mirror. The AOM pattern is generated by a CM2 super computer and the output has a 15 degree viewing angle and 25x25x25mm image volume. The display's output was constrained to be small because any increase in size would require the use of an impractically large rotating polygon. In 1992, the system was upgraded to create three-color images by using a three-channel AOM.

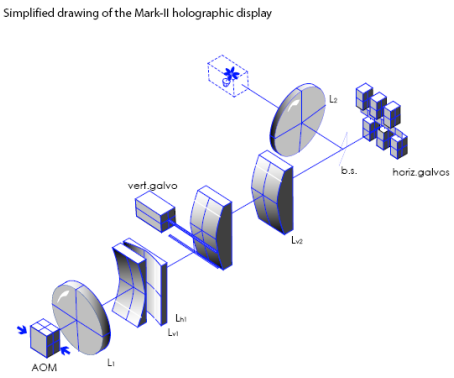

Figure 2-2: The Mark II Holovideo Display

The MIT Mark II, 1994

The second generation MIT holovideo display, or Mark II[22], used an 18-channel AOM instead of a three-channel AOM and a bank of scanning mirrors instead of a rotating polygon. This version of the display could be scaled by simply adding more AOM channels and more scanning mirrors. The Mark II was a six-fold scale-up from the previous display with an image volume of 150x75x150mm (width by height by depth) and a 30 degree viewing angle. The Mark II was driven initially by a custom-built supercomputer called Cheops[26] created at the MIT Media Lab. Recently Bove[9] replaced Cheops with a set of commodity PCs with gen-locked video cards acting as a bank of high bandwidth framebuffers.

The MIT Mark III, 2005

In the Mark III, the *bulk wave* AOM in which acoustic waves travel through the volume of a crystal, has been replaced with a *surface acoustic wave* (SAW) device called a *guided-wave optical scanner* that uses acoustic waves traveling along the surface of the crystal to interact with light confined just beneath the surface in diffused waveguide regions. Lithium Niobate is used for these devices which has a much lower acoustic attenuation than TeO_2 and is useful for modulating light with acoustic frequencies well into the GHz range. The horizontal bank of scanning mirrors is replaced

[1]Figures for the Mark I, Mark II and Mark III were drawn by Quinn Smithwick.

in this generation by a holographic optical element (HOE), rendering the horizontal de-scan entirely solid-state. Together, these improvements make the display easier to scale and more suitable for mass-production.

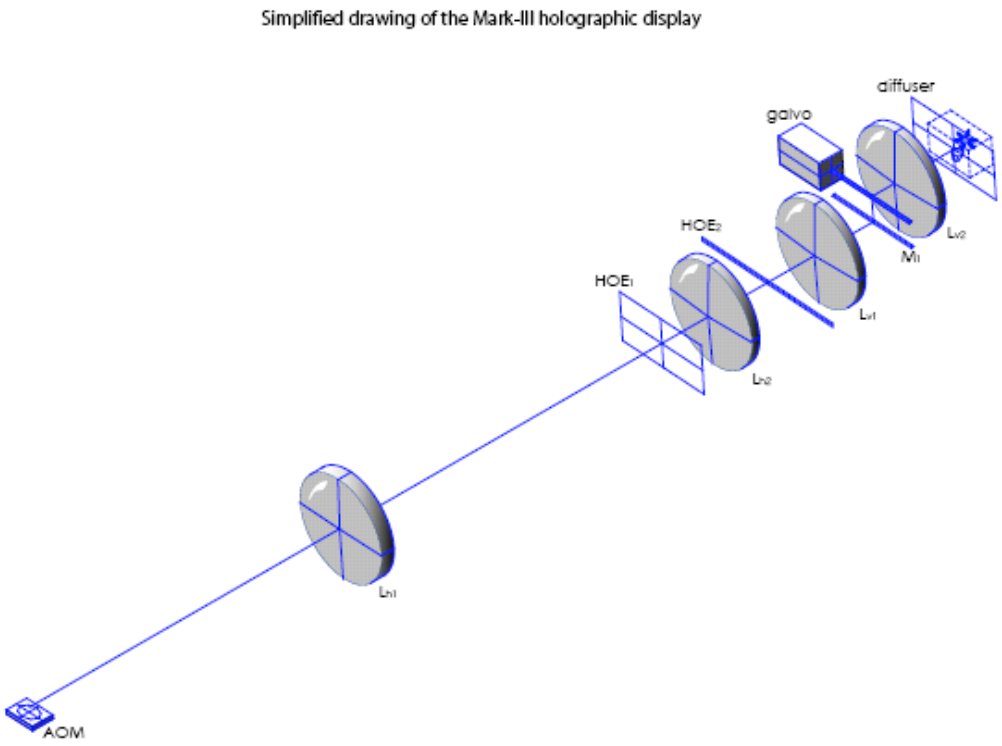

Figure 2-3: The Mark III Holovideo Display

Chapter 3

Mark III Theory of Operation

The proposed improvements to the holovideo geometry are largely understood by applying concepts from diffraction theory and Fourier optics.

3.1 Overview of the Geometry

Before focusing on individual components, let's first review the system-level light path of the Mark III:

Laser light couples into the waveguide of the guided-wave scanner. SAW waves, acting as holographic fringes traveling *orthogonal* to the light in the 'y' direction, cross the guide and modulate the confined light through isotropic Bragg diffraction. Then SAW waves *collinear* to the diffracted light traveling in the 'x' direction rotate the light's polarization and diffract it down and out of one of the crystal's faces. Next, the light travels through a four-f processor with a de-scanning HOE at the Fourier plane. As the guided-wave scanner translates the light vertically, the HOE deflects horizontally so that when the light emerges from the four-f system its holographic information has been de-scanned and appears stationary. A second HOE collimates the light and passes it through a second four-f system, this time meeting a vertical scanning mirror at the Fourier plane and emerging multiplexed vertically to build a screen-sized output. Finally the light travels through a vertical diffuser which creates a vertical focus in space while the light focuses horizontally into points forming a

holographic image viewable by the observer.

With the system-level picture in mind, we can focus on the function of the de-rotation HOEs and the guided-wave scanner.

3.2 Holographic Optical Elements

We would like to replace the bank of fast-scanning horizontal galvos with a static optic. To accomplish this we can leverage the fact that the MIT holovideo system is horizontal parallax only, and try to capture the function of the scanning mirror in time and encode it spatially on a static optic in the vertical direction. In other words, we would like to create an optical element that would work something like this: if you send a laser beam though the top portion of the element, the beam deflects horizontally at some small angle. Then if you send a laser beam through the bottom portion of the element, the beam deflects horizontally at a much larger angle. Finally, if you shoot the laser at some intermediate height you should expect an intermediate horizontal deflection on the output so that by translating the input beam vertically you can expect the output beam to scan horizontally. This sounds simple, but finding an optical element that can do this is not trivial. The key complication is the need for an optical element that modulates light only horizontally and not vertically. For most geometric optics like prisms and mirrors, this cannot be done directly. Consider the illustrative example of the helical mirror.

One way you might try making the element above is to take several long, thin mirrors and stack them, one on top of the other. As you stack you twist each mirror so that each subsequent mirror is slightly more twisted than its predecessor. What you have, then, is a discrete helical mirror that looks something like a DNA molecule. If you try to scan a laser beam up and down such a mirror the output scan jumps horizontally from one angle to another. You can try to make this a smooth scan by having thinner and thinner mirrors but just as the jerkiness of the scan begins to fade, the vertical diffraction effect caused by the thin mirrors starts to take over, smearing the resulting beam in the vertical direction. Another solution might be to

take this discrete version to its continuous limit and make a continuous helical mirror. Such a mirror was designed and built by Dr. Quinn Smithwick (illustrated below). It deflects light smoothly and without diffraction but the reflected light is not just deflected horizontally but vertically as well. The reason for this is that the surface normal of the mirror faces changes from flat to tilted when the mirror goes from discrete to continuous. When this happens the slope of the mirror and the direction of the surface normal become a function not just of y but of x as well.

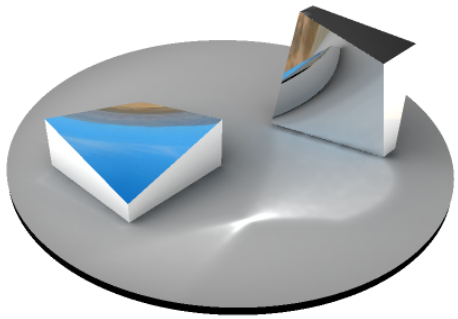

Figure 3-1: A computer generated model of helical mirrors (courtesy of Quinn Smithwick.)

We can use a spatial filter to extract the vertical information from the continuous helical mirror. First we use a four-f processor to relay the image of the helical mirror behind a vertical diffuser. Normally, a collimated laser beam reflecting off of the helical mirror would remain a single beam having one horizontal angle and one vertical angle. When we add the diffuser, light hitting the pair now has one horizontal angle but many vertical angles. Now we can filter all but those light rays which are vertically collimated by inserting a thin horizontal slit at the Fourier plane of the processor. Then we make a hologram of the relayed real image. The resulting hologram deflects light only horizontally. Vertically, the HOE is reconstructing the horizontal slit, so if a very thin slit is used during the hologram recording, the HOE that is produced will diffract very little vertically.

3.3 The Guided Wave Scanner

Five important things are happening in the guided wave 2D scanner: coupling, confinement, surface acoustic wave generation, Bragg diffraction and mode conversion.

3.3.1 Coupling

Laser light enters the scanner's waveguide through evanescent coupling. A right angle prism of high refractive index material (Rutile or Indium Phosphide) sits on top of the waveguide and is pressed until a 'wet spot' appears indicating that there is close contact between the prism and the substrate (even with good contact, there is typically some air gap.) Light focused just below the 90-degree corner, enters the crystal and reflects off its bottom and side faces, back towards the laser source. At the bottom of the prism, evanescent fields extend through the air gap and into the waveguide. The angle of the light entering the prism is adjusted and as it varies the spatial frequency of the light at the boundary of the prism/gap interface changes. This spatial frequency at the boundary is called the propagation constant or the wavenumber, β. The waveguide only allows for the propagation of certain wavenumbers called 'modes'. When the laser is tilted to the correct angle, the evanescent fields couple light into the waveguide where it travels as a mode. Prism coupling efficiencies of 81% or more have been reported[23], but efficiencies of 30-50% are more common in practice. It is also possible, though more difficult, to couple light into the waveguide through an etched diffraction grating on the surface, or by butt-coupling a laser or lens tipped fiber to the edge of the guide. These methods are more economical and better suited for mass-production, but for experimentation, prism coupling is more convenient.

3.3.2 Confinement

The waveguide is formed by 'proton exchanging' the surface of Lithium Niobate. Proton exchange is performed by immersing the Lithium Niobate wafer in a melt of Benzoic Acid. The exchange turns $LiNbO_3$ into $HNb0_3$ which has a much higher extraordinary index of refraction $\Delta n_e = +0.12$ and a slightly lower ordinary index of

refraction $\Delta n_o = -0.05$ [27]. Light can be index guided whenever a high index material is surrounded by two materials of lower index of refraction. $HNbO_3$ is surrounded on top by air with an index $n = 1$ and on the bottom by $LiNbO_3$ with an index $n_e = 2.21$ so TM light is guided in the proton exchanged layer, but TE polarized light is not.[1]

3.3.3 Surface Acoustic Wave Generation

Surface acoustic waves are generated by interdigital transducers through the piezoelectric effect and are subject to various loss mechanisms related both to the IDTs (impedance matching) and to the nature of SAW propagation itself.

Piezoelectric Effect

Piezoelectric crystals can change shape in response to an applied voltage or generate a voltage when a crystal is compressed or stretched. All but one of the non-centrosymmetric crystal classes exhibit piezoelectricity, and half of these do so because they have a dipole unit cell. These dipoles may arrange themselves in a crystal lattice so that the net field in equilibrium is zero, but if an external force perturbs the lattice, stretching or compressing the dipole, the equilibrium will be disrupted and a net voltage will appear across the crystal. Similarly, if a voltage is applied, the dipoles will stretch or compress in response to the field causing the solid to deform. Closely related to piezoelectricity are the effects of pyroelectricity and ferroelectricity. A pyroelectric crystal expands with heat causing dipoles to deform and a electric field to be created. A ferroelectric crystal may have dipoles that can be switched. Lithium Niobate, the material we use to make our Mark III's light modulator, is piezoelectric, pyroelectric and ferroelectric.

[1]Please note that we are using the engineer's definition of TM/TE polarization and not the mathematician's definition. To be explicit, the transverse field is that which is transverse to the plane made by the incident and reflected/refracted rays of light.

Interdigital Transducers (IDT's)

In order to create surface acoustic waves, an interdigital transducer is fabricated on top of Lithium Niobate. When voltage is placed across the electrode fingers, the piezoelectric effect gives rise to stress and strain in the crystal. When the voltage is relaxed, the mechanical energy is released as Rayleigh waves that travel on the surface of the crystal like ripples on water. The interdigital transducer is made of several finger pairs. Each finger pair acts like a point or line source for surface acoustic waves. When several of these finger pairs are placed next to each other, they act like an end-fire antenna array, launching waves only out of the two ends of the transducer. The transducer's center frequency is determined by the electrode period and the bandwidth is a function of the number of finger pairs. Both dependencies are governed by the following relations:

$$f = \frac{v}{2p} \tag{3.1}$$

$$B \approx \frac{1}{n} \tag{3.2}$$

where f is the center frequency, v is the velocity of sound in Lithium Niobate, p is the period defined as one half the acoustic wavelength, B is the fractional bandwidth (bandwidth/center frequency) and n is the number of finger pairs.

Also, electrical to SAW power coupling efficiency goes up with the number of finger pairs, n. This results in a tradeoff between large bandwidth and high coupling efficiency. [2]

Impedance Matching

The interdigital transducer has a complex impedance exhibiting real resistance and imaginary reactance. The transducer is impedance matched when a series inductor

[2]Complex transducers involving chirped periods, or slanted fingers are not limited by the bandwidth relation above and can be made to have both wide bandwidth and a large number of finger pairs for efficient wideband operation.

is used to cancel the capacitive reactance. If the real resistance is not 50 ohms after the inductor is added, a second matching element can be used to bring the total real resistance to 50Ω. The real resistance can be thought of as proportional to the width of the transducer, with shorter transducers having a larger resistance than longer transducers. The goal is to design a transducer that can be matched with a single inductor to a real resistance of 50Ω. We can design such a transducer when we understand which mechanisms give rise to loss in the transducer. In a SAW filter, the real resistance has two components: an ohmic resistance, R_{ohm}, and a radiation resistance R_{rad}. The matching inductor may add some ohmic resistance but this is often small. The value given for the radiation resistance is a closed form equation derived from an equivalent circuit model for the SAW transducer by Reeder[25].

$$R_{rad} = \frac{4k_c^2}{\pi\omega_0 C_g^* W} \tag{3.3}$$

where k_c^2 is the coupling coefficient, ω_0, the angular center frequency, C_g^*, linear capacitance density and W, the SAW acoustic aperture. The ohmic resistance is given as,

$$R_{ohm} = \frac{4WR_s}{N\Lambda} \tag{3.4}$$

where R_s is the resistance per square, N is the number of finger pairs and Λ is the acoustic wavelength.

For non-uniform transducers, like slanted or chirped transducers, there are matrix methods[21][5][20] for determining the radiation resistance. These transducers may be used in future iteration of the guided-wave optical scanner.

In order to design a transducer to be 50Ω when matched, we set the sum of R_{ohm} and R_{rad} to 50Ω and backsolve for the appropriate width, W. Unfortunately as frequency goes up the corresponding W for a 50Ω design goes down and so the diffraction efficiency of the SAW wave produced decreases since the aperture width is the interaction length for diffraction. Tsai proposes an alternate, more sophisticated, design for high frequency transducers that involves a phased array of 50Ω transducers capable of beam steering with frequency to meet the Bragg angle for large range of

frequencies while maintaining a large effective width[25]. Phased transducers have not been investigated thoroughly in this work but we will likely have to use this approach for the higher frequency transducers when getting a uniform output becomes the chief concern. For the present investigation all transducers have been kept simple and uniform.

Loss Mechanisms

The Rayleigh waves should, ideally, propagate without loss on the crystal surface, but, likely because of viscous damping, there is a frequency-dependent attenuation of propagating SAW waves. Lithium Niobate, however, attenuates acoustic waves at a much lower rate than does Tellurium Dioxide (Tellurium Dioxide, as you recall, was used in the AOM for Mark II). For Lithium Niobate the attenuation can be expressed as :

$$Attenuation(dB/\mu s) = 0.88F^{1.9} + 0.19F$$

[2] where F is frequency in gigahertz. For 500MHz, the attenuation is 0.33dB/μs. Contrast this with the acoustic attenuation for Tellurium Dioxide (TeO_2): 3dB/μs @ 500MHz for slow shear mode. More impressive still is the fact that because the wavespeed of the slow shear mode in Tellurium Dioxide is 617m/s, acoustic waves in TeO_2 will be attenuated by 3db after only 0.6mm of propagation while SAW waves in Lithium Niobate, traveling at 3909m/s will not be attenuated by 3db until they have traveled over 39mm for frequencies near 500mHz. Lower attenuation means that it is possible to create displays with larger optical apertures which have greater available image depth.

Additional sources of loss include insertion loss and acoustic diffraction. Insertion loss tends to increase with frequency while acoustic diffraction goes up as the electrode length is reduced (as the effective aperture gets smaller). Diffraction loss may be ameliorated by adjusting the overlap (apodization) of each finger pair to modify the far-field SAW mode pattern. You can eliminate SAW diffraction due to the width of the transducer by apodizing a sinc function (the Fourier transform of the desired

far field SAW pattern) along the length of the transducer. Surface acoustic waves generated and filtered in this way by one transducer may be subsequently filtered again and absorbed by a second transducer making very flexible and efficient passive filters[12] and optical modulators.

3.3.4 Isotropic Bragg Diffraction

SAW waves are made of regions of compression and rarefaction which are capable of two types of diffraction: Raman-Nath (thin-film) diffraction or Bragg (thick-film) diffraction. Raman-Nath diffraction occurs when the thickness parameter Q is much less than one[1].

$$Q = \frac{2\pi\lambda * t}{nd^2 \cos\theta_0} << 1$$

Q is the thickness parameter, t is length of the interaction region, d is the distance between fringes, n is the index of refraction and θ is the angle of incidence. In this regime light meets a brief interaction region made of apertures that diffract light to create multiple orders with a maximum first-order diffraction efficiency of approximately 40.5%[1] for thin binary phase gratings and less, 33.8%, for sinusoidal gratings as dictated by the fourier transform. In Bragg diffraction, light enters a longer interaction region of Bragg-planes where the light is both guided as well as diffracted when it meets the Bragg condition (which means it enters at the Bragg angle). This guidance leads to constructive interference of one order and the distructive interference of all other orders resulting in a single order of diffracted light with a maximum efficiency of 100%. As an interation region becomes longer, and as the resulting diffraction moves smoothly from Raman-Nath to Bragg, the diffraction efficiency becomes greater and the allowable input angle for light becomes tighter. The angle of incident light required for Bragg diffraction is called the Bragg angle.

$$\theta_b = \arcsin\frac{\lambda}{2d}$$

where λ is the wavelength of light and d is the distance between Bragg planes. We

Transducer	1	2	3	4	5	6
Center Frequency (MHz)	310	410	560	760	960	1160
Bandwidth (MHz)	100	100	200	200	200	200
Fractional Bandwidth (%)	32	24	36	26	21	17
Electrode Pairs (n)	3	4	3	4	5	5
Approx. Bragg Angle (deg) (n)	1.44	1.9	2.6	3.5	4.6	5.5

Table 3.1: Horizontal Diffraction Transducers

wish to be operating as much as possible in the Bragg diffraction regime so that we can take full advantage of the higher diffraction efficiency and single-order characteristic of this type of modulation. This means that we must design our transducers with as wide an aperture as is allowable without driving the transducer impedance too low.

Horizontal Array of Transducers

We wish to fabricate a scanner that can diffract light over a large range of angles; 10 degrees is an ambitious but reasonable goal for red light in the Mark III system. 10 degrees of diffraction corresponds to an RF bandwidth of, using the Bragg equation:

$$\delta f = \frac{2v \sin 5deg}{\lambda} = 1.07Ghz$$

(where λ=633nm and v=3909m/s)

We need a transducer that has a bandwidth of 1Ghz. By using a simple uniform transducer with only a single pair of electrodes, $n = 1$, we can achieve the requisite bandwidth by placing the center frequency of the transducer at 1Ghz. The very low number of pairs and the very high center frequency make this an extremely inefficient transducer. Raising the center frequency to 2Ghz and doubling the number of pairs does not help much. We could use a slanted transducer or a chirped transducer but that would add a lot more complexity and still would not be as efficient as using an array of simple transducers as suggested by Tsai[25]. We could break up the requisite bandwidth of 1Ghz into six chunks, two 100MHz chunks and four 200MHz chunks as shown in Table 3.1. Each transducer must be tilted to meet a different Bragg angle.

We could continue to subdivide the bandwidth and make more transducers, but

the hardware driving the scanner has channels with 200Mhz maximum bandwidth, making this 200MHz transducer configuration a desirable match. The first two transducers have been designed with smaller bandwidths to facilitate characterization of the scanner; however, in the next iteration of the device, these first two transducers will be combined to form one transducer with a 200MHz bandwidth and a center frequency of 360MHz.

The holographic information is fed into this array of transducers producing surface acoustic waves that cross the waveguide where laser light is traveling at the Bragg angle for each transducer. Note that light will diffract only once because, once it has diffracted, it will no longer be at traveling at the Bragg angle. Furthermore, the laser illumination angle is adjusted and the horizontal transducers slightly rotated so that diffracted spread of light output travels in the direction of the second collinear transducers where mode conversion of the newly diffracted light takes place.

3.3.5 Mode Conversion

The vertical scan is accomplished using collinear surface acoustic waves that convert the guided TM mode light into leaky mode TE polarized light. This collinear transducer has roughly a 460Mhz center frequency, a 50Mhz bandwidth and is similar to the transducers described above but orthogonally rotated so that the output SAW waves are traveling along the length of the waveguide, 'head on' toward the incoming diffracted light spread. The collinear wave basically diffracts the light down, out of the waveguide and changes its polarization in the process. A slightly better way to think about this interaction is to say that the momentum vector of the acoustic wave is subtracted from the momentum of the diffracted light vector resulting in a light wave with a reduced wavenumber (propagation constant). As we learned earlier waveguides only support light of particular wavenumbers, so if this wavenumber of guided light is changed, then it is no longer guided. Instead the light scatters and since it is scattering from a periodic structure (i.e. the SAW pattern) it has a favored direction and polarization which in this case is down into the substrate with TM polarization (all TE scattered light is trapped in the waveguide where it destructively

interferes with itself and disappears). The most complete explanations require the use of a special case of Haus Coupled Mode Theory[3]. The upshot of this mode conversion is that, by varying the frequency on the collinear transducer we can scan the diffracted light vertically as it drops out of the waveguide and exits the crystal. This vertical deflection becomes an extra degree of freedom that we can use to perform the horizontal de-scan.

3.4 System Assumptions

In using the guided-wave scanner and the HOE solution, we make the assumptions that sufficient light can be coupled into the device to produce display level brightness on the output. The output of the display is highly directional compared to other displays so the requirements for power are somewhat looser, however there is significant loss at the guided-wave device. There will be a considerable loss of light when it is coupled into the waveguide, and at least half the light will be lost at the horizontal diffraction step and another half will be lost during the collinear TM/TE coupling step. These losses by themselves should be tolerable considering the fact that the noise will be eliminated by polarizers. Care will need to be taken to reduce the total number of external interfaces and other diffractive losses in the HOEs adding to the total system loss.

It is also assumed that the change of frequency of the collinear interaction will be fast with respect to the angular change of the helical mirror so that only one effective angular view will be addressed at a time, otherwise a loss of views or overlapping of views may result. However, even if it does turn out that more vertical resolution is needed, the interaction length used by the vertical scan can be increased to add vertical resolution.

3.5 Relevant Literature

Many of the papers most relevant to the function and design of the guided-wave scanner are found in the book "Guided-Wave Acousto-Optics" edited by Tsai[25] [24] though the device appears in its rudimentary form in early works [18]. Tsai's book describes in some detail the design of waveguides and transducers (both simple and phased) for use in guided wave devices.

The literature most relevant to the holographic video geometry includes Dr. St.-Hilaire's PhD Thesis on the Mark II system, [22] and those theses that predate his work [8],[10].

Chapter 4

Fabrication of the Guided-Wave Scanner

The fabrication of the guided-wave scanner involves four steps: making the mask, forming the waveguide, patterning the transducers and matching the device impedance to the drive impedance.

4.1 Mask Making

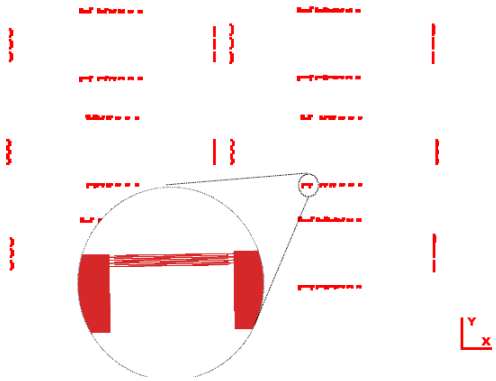

Figure 4-1: Mask design with closeup of one transducer.

For the purposes of this research, it makes more sense to use a contact mask for patterning transducers. The alternative would be to use a stepper mask, but

to have such a mask made at the resolution we require (0.8μm) would be too expensive, especially when it is likely that we will only use the mask a few times before modifying the transducer design. Furthermore, contact masks can give better resolution than even stepper masks when there is a conformal contact between the mask and the Lithium Niobate substrate. The mask pattern used for fabricating guided-wave scanners is shown in Figure 4-1.

The process flow for the fabrication of a contact flex mask is given below. All of the fabrication steps were performed at either the MIT Media Laboratory, Nanostructures Laboratory (NSL), Scanning Electron Beam Laboratory (SEBL) or in the Experimental Materials Laboratory (EML) of the Microsystems Technology Laboratory (MTL).

Process Flow

Start with a clean Fused-Silica or Quartz wafer, 200-300nm thick, 3in (76mm) diameter. (Mark Optics Inc. Santa Ana, CA)

1. Spin 3.5% PMMA at 3000 RPM, NSL/EML
2. Bake on a hotplate for 2min at 150°C, NSL/EML
3. Deposit 8nm Chrome, NSL/EML
4. Ebeam Write, SEBL
5. Etch Chrome CR-7, NSL/EML
6. Develop in 2:1,IPA:MIBK, NSL/EML
7. Evaporate 150nm Chrome, NSL/EML
8. Lift-off Chrome in Acetone or Chlorobenzene NSL/EML

4.1.1 Mask Material and Thickness

Conformal contact requires that either the substrate or the mask be thin and that any air between the mask and substrate be removed by vacuum. In our case the substrate must be thick and the mask thin because light must have room to exit from the wafer's edge. I use three-inch (76mm) UV grade quartz or UV fused silica substrates between 200μm and 500μm thick. The UV rating is not strictly necessary for i-line work, but having the option to move to a smaller wavelength may become more important as we progress toward transducer designs that are more sophisticated, such as designs involving phased or slanted transducers.

Thin Quartz is fragile enough that if the edge of the wafer is nicked, the mask will likely crack during later processing steps. Try to handle the wafers with freshly-gloved hands as often as possible, and when this is not possible, take care not to pinch the wafer when using tweezers.

Unless you are sure that the wafer has been pre-cleaned, it would be wise to solvent clean it by rinsing it first in Acetone, then in Methanol and finally in 2-Propanol. For a more energetic removal of organics, clean the wafer using *Piranha*, which consists of one part Hydrogen Peroxide to five parts Sulfuric Acid, in an acid hood for 15 minutes. Rinse the wafer with de-ionized water and then dry with clean, compressed air.

4.1.2 Spin 5% C PMMA, Poly(Methyl Methacrylate)

950 PMMA Poly(Methyl Methacrylate) 5C is available from MicroChem in Newton, MA. The spin curve is shown below: I mix a 3.5% dilution of PMMA in Chlorobenzene and spin it onto the substrate at 3000rpm for one minute to obtain a 400nm layer. For lift-off, it is desirable to have a resist layer that is at least double the thickness of the material to be deposited. It is desireable to have as thin a layer as possible so that your small features are not patterned with too high an aspect ratio (thickness to width). Since our final mask metal layer is 150nm thick, and our minimum feature size is approximately 800nm, a 400nm resist thickness is adequate to facilitate lift-off

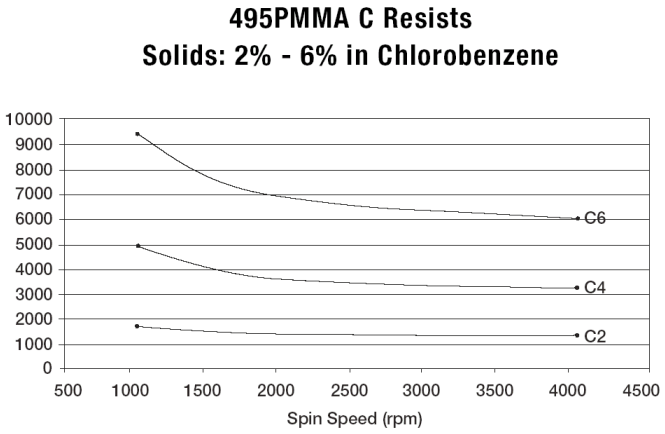

Figure 4-2: Spin curve for PMMA (MicroChem)

while maintaining a low aspect ratio for small features.

4.1.3 Bake on a hotplate for 2min at 150°C

With most photoresists, it is important that you bake the resist to above the solvent boiling temperature (the boiling point of Chlorobenzene is 132°C) and the glass-phase transition temperature of the resist (105°C for PMMA[19]). The online documentation for PMMA suggests a hotplate bake of 60-90sec at 100°C, however, baking at this temperature has produced poor quality resist layers that degrade immediately in developer with or without exposure. Use the higher temperature of 150°C given above and, if possible, use a hotplate with vacuum contact to ensure even heating of the wafer.

4.1.4 Deposit 8nm Chrome

It is necessary to deposit a thin metallic layer above the resist to act as a Faraday Cage for charge accumulated from the ebeam write that becomes trapped in insulating materials like Quartz or Lithium Niobate. Typical shielding layers have thicknesses ranging from 5-8nm.

4.1.5 Ebeam Write, SEBL

Initially, I tried two approaches to writing the mask pattern. The first approach used a Heidelberg laser writing tool and the second approach used the VS26 ebeam tool. The Heidelberg is nominally capable of writing sub-micron features, but even after several months of adjustment and testing we were unable to produce a suitable mask. The ebeam writing tool, on the other hand, had more than sufficient resolution for the transducer patterns. The ebeam write times are rather long (several hours) but the quality is very high. The ebeam's high resolution was especially important for patterning tilted transducers because these patterns were approximated by the juxtaposition of several lines with widths as small as 25nm.

The VS26 ebeam tool, run by Mark Mondol of SEBL, uses VXF files converted from a master .kic file. Most layout editors I encountered had difficulty creating .kic files for structures with slanted features, like the horizontal array of transducers tilted at the Bragg Angle. A special MATLAB (Mathworks, Natick, MA) library called, Matkic, was created by Chris Dames of the MIT NSL specifically for the purpose of creating non-manhattan .kic geometries. Matkic was used to create the horizontal transducers and the rest of the mask editing was done in Nanowriter, a program written by Mitch Meinhold of the NSL.

Table 4.1 gives typical parameters for an ebeam run.

Table 4.1: Ebeam Write Parameters

Field Strength	50kV
Dose	426μC
Bias Current	2nA
Write Speed	750kHz
Field Size	406.9μm
Number of Pixels	2^{28}

My straight-lined pattern, covering 2cm by 5cm took two hours. The same pattern with slanted features approximated by off-center boxes took 4 hours.

4.1.6 Etch Chrome CR-7, NSL/EML

Before the exposed mask can be developed, you must first remove the thin Chrome layer with CR-7 etchant. The Chrome disappears within a few moments but I keep the wafer in the etchant for at least 30 seconds to make sure that no Chrome remains.

4.1.7 Develop in 2:1 IPA:MIBK, NSL/EML

PMMA may be developed in a solution of Isopropyl Alcohol (IPA) also called '2-Propanol,' and Methyl Isobutyl Ketone (MIBK) in a 2:1 IPA to MIBK proportion. These are generally mixed by weight, and I would suggest that you mix a liter or so at a time. According to Mark Mondol of the SEBL, the mixture of the two liquids causes an endothermic reaction that drops the temperature and temporarily reduces the solution's effectiveness as a developer. It is necessary to wait for the solution to warm to room temperature before continuing with the development step.

4.1.8 Evaporate 150nm Chrome, NSL/EML

In order for a mask to be opaque enough to faithfully transfer the desired pattern, the Chrome areas must be several 'skin-depths' thick. The skin depth, δ, is the depth required for incident light to be attenuated by $1/e$. For a good conductor like Chrome, δ is:

$$\delta = \frac{1}{\Im(k)} = \sqrt{\frac{2}{\omega\mu\rho}} = 6.3nm$$

where ρ is the conductivity of Chrome, $\rho = 7.7 * 10^6$ S/m and μ is the permittivity of freespace, $\mu = \mu_0 = 4\pi 10^7$H/m and ω is angular frequency of the incident light, $\omega = 2\pi f, f = 8.3THz$ and $\Im(k)$ is the imaginary part of the wavenumber k.

If the skin depth is 6.3nm, a Chrome layer of 150nm can be considered opaque.

4.1.9 Lift-Off Chrome in Acetone or Chlorobenzene NSL/EML

Chrome covered PMMA lifts off in Acetone, but not as well as other resists. Mark Mondol uses Chlorobenzene for the lift-off solvent. Do not sonicate for more than a few seconds without checking your pattern under a microscope. Ultrasonic energy delivery goes proportionally with the length of the features, and SAW transducers often have electrode fingers as long as a millimeter.

4.2 PE Waveguide Design, Fabrication and Analysis

For our research we chose to use proton exchange over the method of Titanium indiffusion for the creation of waveguides. Titanium indiffusion does not produce as high a change in index of refraction and it requires very high temperatures, over 1000°C compared to 200°C for proton exchange. Proton exchange is a less complicated process, in which the substrate is simply immersed in a melt of acid. proton exchange does have some disadvantages such as time instability and poor nonlinear properties, but these are not immediately important for our application.

Several acids have been used for proton exchange—Sulfuric, Octanoic and Benzoic—but Benzoic has been the most popular due to its relative safety over Sulfuric acid and relative speed of exchange over Octanoic acid.

4.2.1 Waveguide Design

We want a single mode guide with enough confinement for effective diffraction within the waveguide. Too large or too small a waveguide thickness will result in poor overlap between sound and light waves. Tsai suggests using a waveguide depth of 1μm.[3]

The literature has reported that PE waveguides have a step like profile and can be described using the following diffusion constants, $D = 0.44\mu^2 m/hour$ for Z-cut Lithium Niobate at 236°C.

Acid	Temp (°C)	Time (hrs)	Thickness (μm)	Index ChangeΔn
Benzoic Acid	200°C	4	1.24	0.1
Benzoic Acid	200°C	12	1.5	0.1

Table 4.2: Waveguide index and thickness for common bake times and melt temperatures.

4.2.2 Waveguide Fabrication

Below is the process flow for the fabricating light guides on the surface of a Lithium Niobate substrate.

Beginning substrate: Z-cut Double-Side Polished Lithium Niobate, 1mm thick (least expensive), 3in (76mm) diameter. (Crystal Technology Palo Alto, CA)

1. PECVD 250nm $Si0_2$, EML
2. Spin negative photoresist (Futurrex NR8-1000P), bake 15min at 100°C, NSL
3. Expose UV source to an energy of 40mJ, NSL
4. Develop in 2% R2 developer, NSL
5. Buffered Oxide Etch 1min, solvent clean, NSL
6. Proton Exchange, Benzoic Acid, Acid hood 200°(time is variable)
7. Buffered Oxide Etch, Acid Hood, NSL

4.2.3 Waveguide Analysis

Before proceeding with the fabrication of transducers, it is important to verify that a waveguide exists and that it extends to a depth exceeding 1μm. This verification is performed by prism coupling.

Prism Coupling

The values shown in Table 4.2 were measured by a Metricon Model 2010 Prism Coupler. A half wave plate was introduced to allow for TM measurements. This technique relies on mapping the angular position of M-lines.

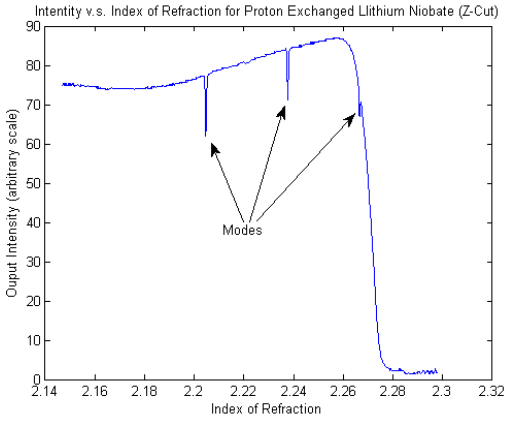

Figure 4-3: Data from the Metricon Prism Coupler. The dips in intensity indicate modes in the waveguide. Each mode 'sees' a different effective index of refraction shown on the x axis in the figure.

When mounting the prism, a 'wet' spot will appear where the prism is in close contact with the substrate. If the wet spot does not appear, twisting the substrate slightly may improve the contact. The Metricon will scan the prism angularly and record the intensity falling on a detector. The Metricon software fits the data to a model waveguide having a particular index of refraction and thickness. Figure 4-3 gives shows the intensity profile and Table 4.2 gives the thickness and index change for two waveguide samples.

4.3 Patterning Transducers

Once the waveguide is in place, transducers can be patterned on the wafer.

start with Lithium Niobate wafer (Z-cut):

1. HMDS 1min/spin 1min/ air-out 1min
2. Spin (NR8-1000P) resist 3-4krpm
3. Bake at 100°C for 15min
4. Expose with i-line using a vacuum chuck
5. Develop in R2 developer for 2min (usually 1:45min clear time), rinse w/water

6. Ebeam deposit 200nm Aluminum

7. Lift-off in Acetone (soak 15min, sonic clean for 10sec)

4.3.1 HMDS

HMDS aides the adhesion of photoresist. To apply HMDS I first use a dropper to completely cover the wafer and wait one minute. Then I spin at some arbitrary speed (3krpm) for one minute and finally let the wafer sit for one additional minute to give time for the HMDS fumes to dissipate.

4.3.2 Spin

NR8 is a negative resist sold by Futurrex Inc. in Franklin, NJ. I have found that it spins to roughly a thickness of 1300nm for 3000rpm or a 1100nm for 4000rpm. When using a transparent substrate like Lithium Niobate you may want to scratch a symbol with no symmetry planes (e.g. the letter 'f') on the photoresist surface to help you keep track of which surface is 'up'.

4.3.3 Bake

The NR8 is prebaked at 100°C for 15 minutes. I have done trials with shorter times, 5 and 10 minutes, and the only real change that I can identify is that the time it takes for unexposed resist to clear becomes shorter when the resist is baked for less time.

4.3.4 Expose

For small features, less than 3 microns, you need good contact between plate and wafer. The i-line aligners are sufficient if there is vacuum contact between the substrate and the mask. I expose for 40 seconds at power of 5mW for a total exposure energy of 200mJ.

4.3.5 Develop

NR8 is developed using R2, a TMAH based developer from Futurrex. The time for unexposed feature to clear varies from 1.5 to 2.5 minutes depending on prebake time and exposure.

4.3.6 Ebeam Deposition

I use an ebeam evaporator for depositing Aluminum. I deposit at slightly less than 4 angstroms/sec at a pressure of $3 * 10^{-6}$ Torr.

4.3.7 Lift-off

Normally, I find that just soaking the wafer in Acetone is not enough to effectively remove all unwanted Aluminum (though this may not be the case with Chrome which seems easier to lift-off). To remove the remaining resist, I ultrasonically clean the wafer for 10 seconds. You may try longer ultrasonic cleaning times, but check the pattern frequently to make sure you are not losing some of your smaller features.

4.4 Packaging

4.4.1 Diesaw

The finished wafer is cut on the diesaw. Photoresist might be used at this step to protect the smaller features from debris that may be circulating over the wafer during cutting.

4.4.2 Mounting and Wirebonding

Each die is mounted on a glass slide and sits straddled by two semicircular pcb boards with radial striplines leading to SMA connectors. The die needs to sit on a flat surface because a prism will later be clamped onto the device for testing and

any bumps underneath the die may cause fractures. The width of the striplines are computed to have a 50Ω impedance.

4.5 Impedance Matching

In order to achieve maximum power transfer to the device and to minimize RF radiation into the air, it is necessary to match the device impedance to the drive impedance. The guided-wave scanner's transducers are impedance matched to 50Ω. For transducers designed to have a real impedance of 50Ω, the complex reactance can be eliminated by using a single lumped-element inductor. All other transducers can be matched with an 'L' network made of one series inductor and one shunt capacitor. The L network has its own resonance peak and it may reduce the bandwidth of the transducer. Once the devices are more fully characterized, all future transducers will be designed to have a real impedance of 50Ω.

At frequencies above a 1 GHz, the quasi-static region is tens of centimeters and as a result care must be taken to account for the length of the cables leading from the network analyzer to the device under test. Ideally, the network analyzer would be calibrated right up to the wire bonds leading to the device. In order to accomplish this, I use the following approach. I make several copies of the pcb board. On the first board I short the leads, on the next I leave them open and on a third board I place a 50 Ω termination. These boards become a calibration kit for the network analyzer. On the remaining boards I place a 50Ω termination and either a series inductor or a shunt capacitor. Then I check to make sure that the reactance shown by the network analyzer is correct for the inductance or capacitance I chose for the board.

4.6 Finished Device

The finished device has 12 ports: 5 horizontal inputs, 5 horizontal outputs, one vertical input and one vertical output. The output ports are not strictly necessary to the function of the scanner but they help sink the acoustic energy that would

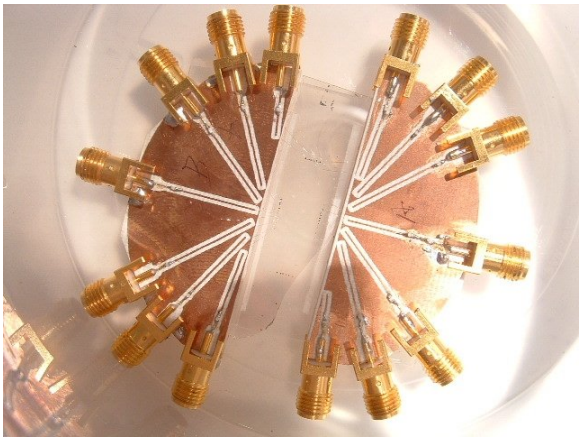

Figure 4-4: Finished Guided-Wave Scanner

otherwise turn into heat and make it easy to monitor the SAW signal while the device is operating.

Chapter 5

Testing and Analysis

The guided-wave scanner has successfully demonstrated coupling, confinement, SAW generation, Bragg diffraction and mode-conversion. However, we were not able to both diffract and mode-convert light simultaneously due to an error in the specification of the collinear transducer center frequency. We observed diffraction from the first two horizontal transducers but any diffraction from the higher frequency transducers was too weak to detect at moderate power levels. Straightforward changes in the device design are proposed below to fix the collinear transducer and improve the diffraction efficiency of high frequency, orthogonal transducers.

5.1 Objective

The guided-wave device must meet its design criteria before it can be used in the Mark III display. The guided-wave device must exhibit coupling, confinement, SAW generation, Bragg diffraction and mode conversion. The target composite bandwidths for Bragg diffraction and mode-conversion are 1GHz and 50MHz respectively. The target range for diffraction efficiency is 10-50% for the horizontally deflecting transducers and 5-10% for the vertically deflecting transducers.

5.2 Procedure

5.2.1 Electrical Measurements

The electrical measurements were performed on an Agilent Network Analyzer. Two plots were generated for each matched transducer: a Smith Chart plot and a Standing Wave Ratio plot.

The Smith Chart is used primarily to aid impedance matching, but it may also show where the acoustic response lies in the frequency spectrum. The SAW transducer acts like a capacitor and follows the imaginary reactance line until it approaches the stop band where its real resistance changes as the transducer begins to radiate acoustic energy. The frequency at which this change peaks should, to a first approximation, be the center frequency of the device.

The SWR plot gives the voltage standing wave ratio,

$$\frac{1+\Gamma}{1-\Gamma}$$

where Γ is the amplitude of the reflected wave. We can find the half-amplitude bandwidth of the transducer by looking at the portion of the SWR below,

$$\frac{1+0.5}{1-0.5} = 3$$

or for half-power bandwidth,

$$\frac{1+(1-.707)}{1-(1-.707)} = 1.8289$$

.

5.2.2 Optical Measurements

Prism couplers were use to introduce light into the guided-wave scanners, while a light meter detected the diffracted and mode-converted output.

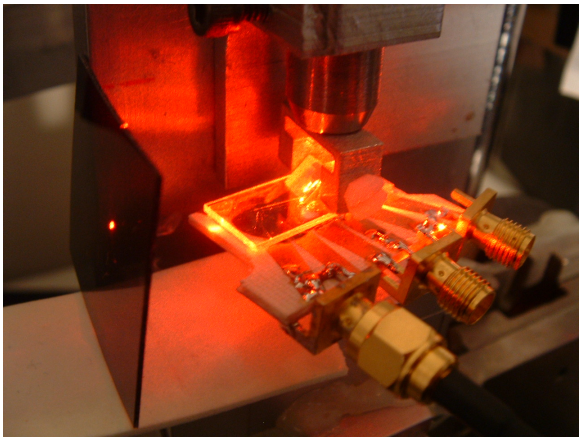

Figure 5-1: Rig for optical measurements.

5.2.3 Coupling and Confinement

Light was coupled into the waveguide with a Rutile Prism. The light was focused to a spot about one tenth of a millimeter in diameter at the 90° corner of the prism. The illumination angle was adjusted until a waveguide mode was excited. The coupling was verified visually by the appearance of a light streak in the guide that would stop when it encountered a scratch or some other surface defect. Substrate modes were also excited but these modes continued to propagate past surface scratches. The coupling efficiency was estimated by measuring the light coupled out through a second prism.

5.2.4 SAW Generation

Each SAW transducer was fabricated so that it would face another transducer on the other side of the waveguide with the same center frequency. To verify that the transducer was radiating SAW waves, the output of the receiving transducer was monitored on an HP8590A Spectrum Analyzer.

5.2.5 Bragg Diffraction

Confined laser light was coupled out of the waveguide using a second Rutile prism. Light appearing next to the zero-order output that moved in response to a changing drive frequency was considered diffracted light. The diffracted light and zero order

light were measured independently with a Newport 840 Optical Power Meter. The diffracted efficiency was determined as the ratio of the diffracted light power to the total (diffracted plus zero-order) light power.

5.2.6 Mode Conversion

There are some inconsistencies in the papers written about TM-TE mode-coupling regarding the appropriate center frequency for mode-conversion. Initially, we tried to reproduce work that specified a vertical transducer center frequency of 360MHz, but we were unable to get polarization-rotating mode-conversion. Later papers suggested that this frequency ought to be higher—460MHz for 1μm deep waveguides. In order achieve mode conversion with an existing device, a guided-wave scanner was turned on its side and a laser beam was coupled into the device so that the horizontally deflecting transducers that are typically orthogonal to the beam were now situated collinear with the guided light. The guided beam was aimed at the second horizontally deflecting transducer, centered at 410Mhz and the light exiting through the side face of the device was observed through a sheet of polarizing film. Any light that exited with a TE polarization and responded to a changing drive frequency was considered mode-coupled light.

5.2.7 HOE

The HOE was made holographically on a floating Newport table using 632.8nm light from a Helium-Neon laser. The layout for recording the HOE is shown in Figure 5-2 below. The recording material is AGFA 8E75 which is exposed to an energy of approximately 60μJ/cm^2. The HOE is made using a 1:1 object to reference beam ratio for maximum diffraction efficiency.

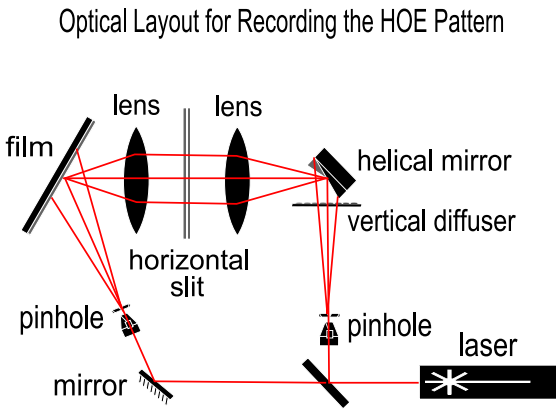

Figure 5-2: Layout for the recording of the horizontal de-scan HOE.

5.3 Results

5.3.1 Coupling

We can routinely couple 10 to 30 percent of incident laser light into the proton-exchanged waveguide. We have also been able to choose the mode of propagation by changing the angle of light input as shown in Figure 5-3. The first mode corresponds to the lowest angle of incidence. For each additional mode a higher angle of incidence is required until the critical angle for the $HNbO_3/LiNbO_3$ is reached.

5.3.2 Confinement

Confined laser light forms a bright streak as it propagates in the waveguide. Light coupled out of the waveguide forms a series of noisy bands, called m-lines. The m-line corresponding to the propagating mode has a bright spot in the center. As the light propagates, it scatters off imperfections in the waveguide. This scattering can be seen as a background haze surrounding each mode spot.

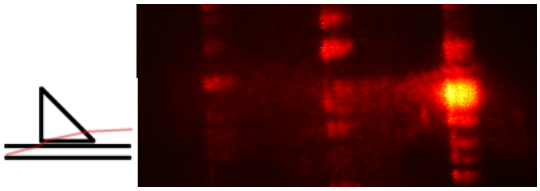

(a) First mode

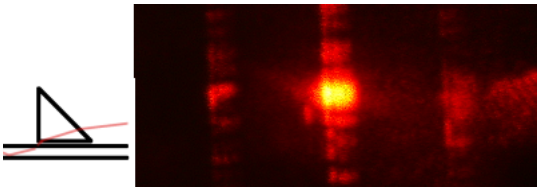

(b) Second mode

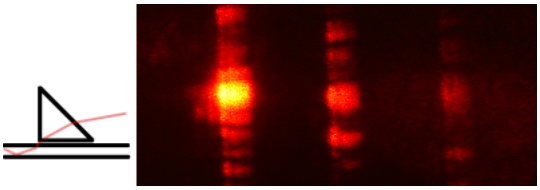

(c) Third mode

Figure 5-3: Waveguide Modes

5.3.3 SAW Generation

Transducer Array

Design and experimental data for a guided-wave scanning device are summarized in Table 5.1. From the table we can make several observations about the device. First, the electrical bandwidth meets or exceeds the design specifications for those transducers that were successfully matched. Second, the transducer center frequencies were off by 10-15% and the diffraction efficiency dropped to an undetectable level for higher frequency transducers. Finally, the most unexpected result was the widely varying resistance values for transducers that were designed to all have the same resistance.

Transducer Center Frequency

We expect the transducer's peak frequency response to occur at the transducer's respective center frequency, but this is not the case for all of the transducers described

Transducer	H1	H2	H3	H4	H5	H6	V1
Design Center Frequency (MHz)	310	410	560	760	960	1160	360
Actual Center Frequency (MHz)	328	444	560	760	–	–	360[1]
Design Bandwidth (MHz)	100	100	200	200	200	200	50
Actual Bandwidth (MHz)	100	140	221	320	–	–	65
Diffraction Efficiency (%)	10	1	–	–	–	–	–
Design Resistance (Ω)	13	13	13	13	13	13	13
Actual Resistance (Ω)	46	39	11	12	–	–	14
Matching Inductance (nH)	105.6	70.2	56	15	–	–	50

Table 5.1: Horizontal Diffraction Transducers

in Table 5.1. The first two transducers have a peak frequency response that is higher than their nominal center frequency.

Transducer Electrical Bandwidth

According to the SWR plots (Figure 5-5), the half-amplitude bandwidth is equal to, or greater than the design value for matched transducers.

Resistance Variation

The width of each transducer in the array was designed to have approximately 13Ωs of radiation resistance. The measured transducer resistances were 46Ω, 39Ω, 11Ω, 12Ω and 14Ω.

5.3.4 Maximum Diffraction Efficiency

Bragg diffraction was observed for the first and second horizontally deflecting transducers. The diffraction efficiency was moderate for the first transducer and poor for the second. At some angles we see two diffracted orders instead of one as shown in Figure 5-6.

Diffraction was undetectable at moderate drive powers for horizontally deflecting transducers above 500MHz center frequency.

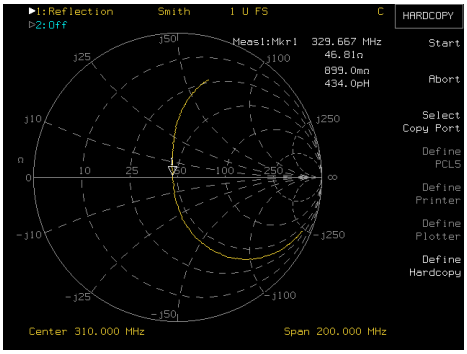

(a) The H1 transducer, nominally centered at 310MHz, but the peak response is actually centered near 328Mhz.

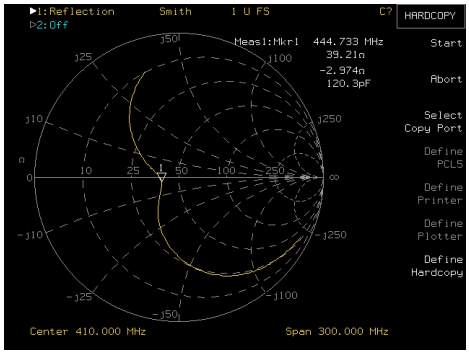

(b) The H2 transducer, nominally centered at 410MHz, but the peak response is actually centered near 444Mhz.

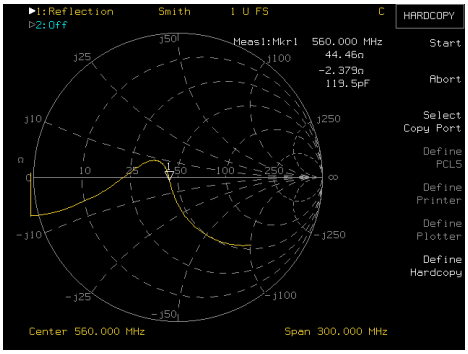

(c) The peak response for the 560MHz transducer is not easily seen from this plot, since the impedance becomes aberrant for high frequencies.

Figure 5-4: Smith Chart plots of impedance for the first three horizontally-deflecting transducers

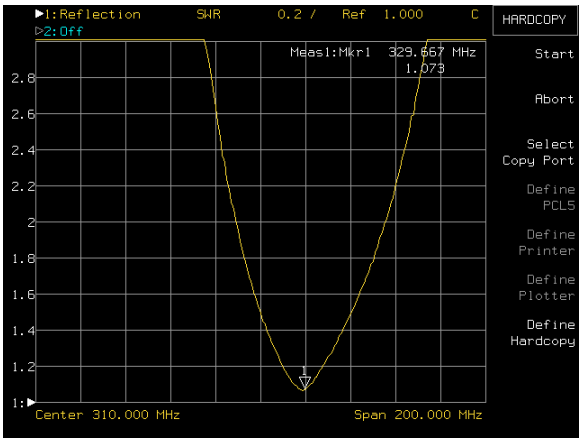

(a) The H1, nominal 310MHz transducer, has an electrical bandwidth of just under 100Mhz.

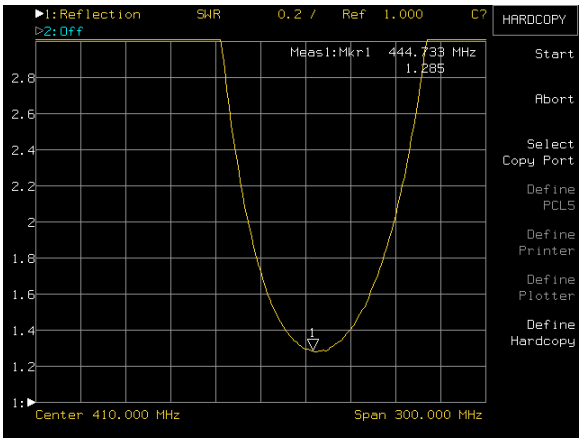

(b) The H2, has a bandwidth of over 140Mhz. Notice that the span for this plot is 300MHz not 200MHz like the plot for H1.

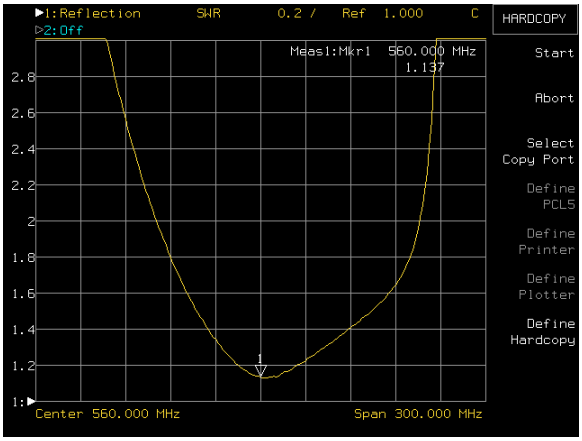

(c) The H3, transducer appears to have a bandwidth of 221MHz.

Figure 5-5: Standing Wave Ratio (SWR) plots for the first three horizontally-deflecting transducers.

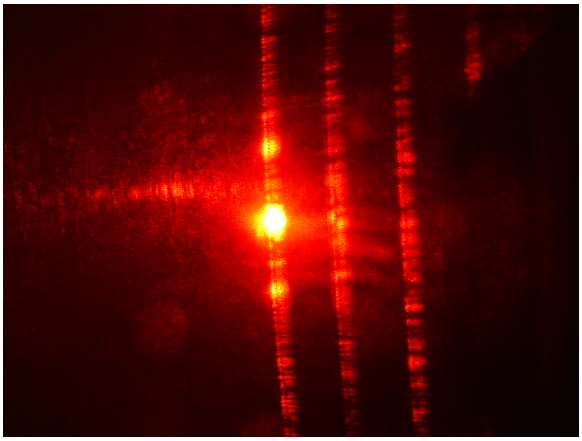

Figure 5-6: The fact that there are two diffracted orders means that the SAW waves are still in a thin-film, Raman-Nath regime. The power of the SAW waves could be increased or the transducers could be made longer to bring the diffraction into the Bragg regime.

5.3.5 Mode Conversion

As explained in section 5.2.6 we tested mode conversion by turning the device on its side and by using one of the horizontal transducers, centered at 410MHz. In this non-ideal configuration, we did see polarization-rotated mode conversion over a small angle. Figure 5-7 shows the mode coupled light viewed with and without a polarizer.

5.3.6 HOE

The HOE output is shown in Figure 5-8. The HOE output was photographed three times. Each time the laser position was incremented vertically. The three resulting photographs where superimposed to form a composite picture. The bright zero order in the middle is straddled by the diffracted orders that move in and out as the laser illumination is translated up and down. The diffracted orders are surrounded by a slit-shaped haze. The first order diffraction was measured to be less than 30%.

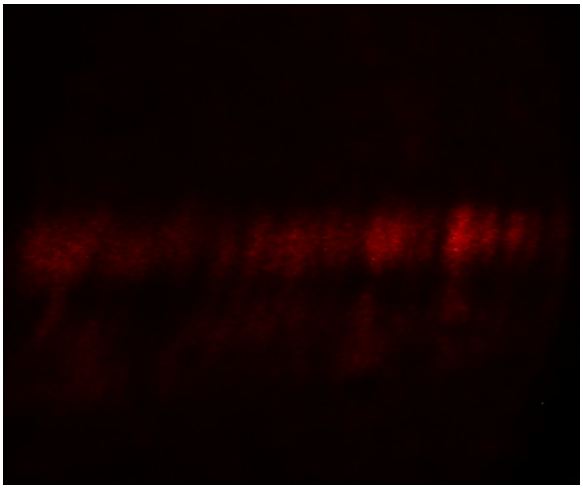

(a) Mode converted light in noise.

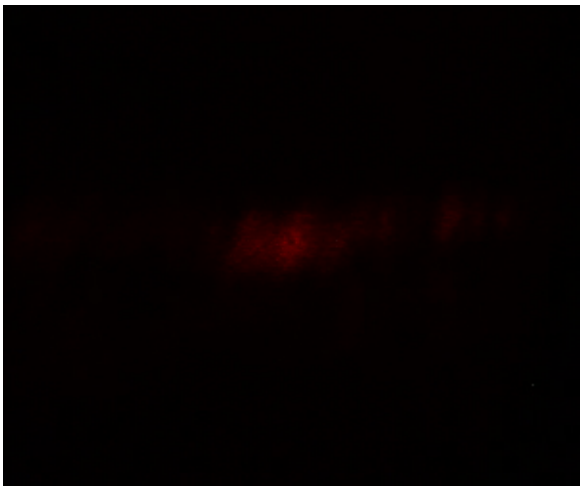

(b) Mode converted light passed through a polarizer.

Figure 5-7: Mode coupled light viewed with and without a polarizer.

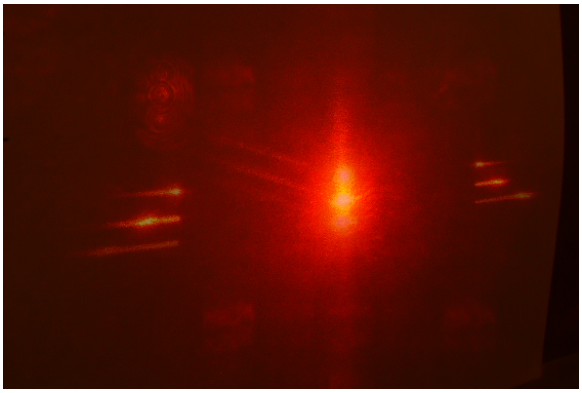

Figure 5-8: Superposition of three images of the HOE ouput, each taken with the illumination laser at a different height.

5.4 Discussion

5.4.1 Coupling

Prism couplers are convenient and effective tools for coupling light, but they are made of expensive materials chosen for their high index of refraction. Eventually, if the devices are to be made part of a mass-produced display, they will have to employ another method of coupling. Once the other functions of the device are well characterized and we have achieved our target bandwidth for vertical and horizontal diffraction, we will begin an investigation of less expensive coupling structures, like those designed by Yuichi Handa[6], that can be built directly onto the device during fabrication.

5.4.2 Confinement

The noise observed around the output beam is a result of light scattering off imperfections in the waveguide. Unfortunately, some of this light will have its polarization rotated during mode-conversion along with the holographic information and will not be extracted with the rest of the noise. It is possible that this waveguide scatter can be reduced by post-annealing or by diluting the Benzoic Acid.

5.4.3 SAW Generation

Transducer Center Frequency

The first two transducers have a peak frequency response that is higher than their nominal center frequency. This suggests that the actual SAW velocity may be higher than the velocity used to calculate the finger period. Another possibility is that second order effects like electrode self-reflection are significant, making our first-order assumption—that the peak frequency response will center around the center frequency—invalid. If this is the case, it may be necessary to use a more sophisticated modeling method, like a matrix method, in order to obtain a better design

agreement in future iterations. For the present, it is sufficient to modify the electrode period slightly to obtain the correct center frequency.

Transducer Electrical Bandwidth

The measured net bandwidth is also a function of the impedance matching circuit. The matching circuit may have a passband that is either narrower than that of the transducer or that is shifted in the spectrum with respect to the transducer's passband. Since the bandwidth values for matched transducers meet or exceed the device specifications, these variations from the expected bandwidth are not worrisome.

Resistance Variation

Some of the variation in resistance that we observed may be due to the contribution of ohmic loss to the real resistance. This would explain why the resistances are not all the same, since ohmic losses would, contrary to intuition, add smaller and smaller values for electrodes of higher and higher frequency. Narrower electrodes on high frequency transducers would have a higher resistance than those on lower frequency transducers, but the resistance is inverted as part of a transformation in the matching step.

5.4.4 Maximum Diffraction Efficiency

The fact that there were two diffracted orders instead of one for some illumination angles means that either the interactions region is too short or the power density is too low for the diffraction to be entirely in the Bragg regime. More Bragg-like diffraction and higher diffraction efficiency should be possible with higher drive powers and longer electrode fingers (i.e. longer interaction length) for the first two horizontally deflecting transducers.

The fact that diffraction was undetectable for transducers three through six suggests that simple uniform transducers are not effective for frequencies above 500Mhz. On Y-cut Lithium Niobate, simple transducers can be used until center frequencies

reach 1GHz, however, since the Z-cut wafer has only one third the electro-mechanical coupling efficiency available to Y-cut[27], it makes sense, then, that we can only go to roughly a third of the frequency obtainable in the Y-cut material before having to resort to phased transducer designs.

5.4.5 Mode Conversion

The next iteration of this device will have vertically deflecting transducers with the higher, 460MHz, center frequency. With this center frequency correction we should expect to see polarization-rotating mode coupling from the vertically deflection transducers.

5.4.6 HOE

The HOE is noisy. The fact that there is noise around the zero order suggests that there may have been plate fogging before or after the exposure. Additionally, the visibility of the slit may mean that the object beam picked up a lot of noise when passing through the diffuser and off the helical mirror. A better HOE might be made if the optics were carefully covered so that no unwanted light entered the system. A different emulsion, like Dupont Omnidex Photopolymer, might also make it possible to get higher diffraction efficiency. However, a better long term strategy might be to pursue writing the HOE pattern directly to achieve optimal performance.

Chapter 6

Conclusion/Future Work

6.1 What we've done

We have fabricated a device capable of demonstrating all the underlying phenomena key to the operation of a guided-wave scanner: coupling, confinement, SAW generation, Bragg diffraction and mode-conversion. We have achieved the target electrical and optical bandwidth in the first two transducers. We have also outlined the next generation MIT holovideo display, which possesses a novel solid-state horizontal de-scan and has the potential to be mass-manufactured at low cost.

6.2 Contributions

Both the guided-wave scanner and the HOE de-scan are original contributions. The scanner described in this thesis is, to my knowledge, the first application of guided-wave acoustooptics to macro-scale projection and display. Additionally, the concept of using of a vertical scan coupled with an HOE for optical de-rotation is also a unique contribution in the field scanned aperture electro-holography. These two innovations effectively remove the scaling barrier that limited earlier generations of the MIT holovideo display.

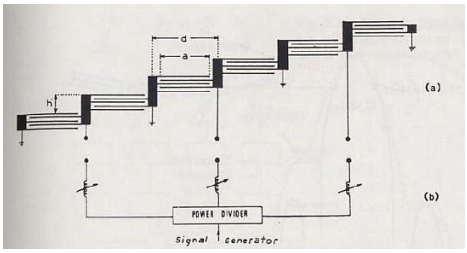

(a) The phased transducer provides a long interaction region for efficient diffraction.

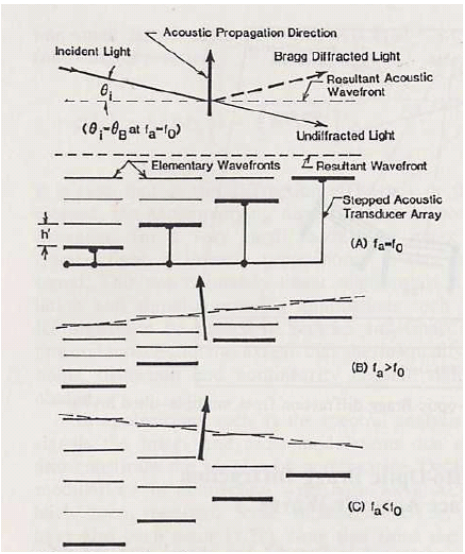

(b) The phased array of transducers can track the Bragg angle as the exitation frequency changes.

Figure 6-1: Phased transducer figures from Guided-Wave Acoustooptics by Tsai.

6.3 Future work

The next iteration of the guided-wave scanner will have a corrected center frequency for the vertical scan, making possible effective mode-conversion and enabling the use of polarizers to reject noise. Also, phased transducers like the one described in Figure 6-1 will replace simple transducers with center frequencies above 560Mhz so that the scanner will be able to diffract efficiently over its entire bandwidth. With these last few challenges overcome, the device, coupled with the de-scan HOE, will be ready for use within the Mark III prototype display.

6.3.1 Fabricated Couplers

Since prism couplers cost approximately $500.00 each, they are not feasible long term solutions for light coupling. A coupler patented by Yuichi Handa, shown in Figure 6-2, would be an ideal coupler for the guided-wave scanner. This coupler could be made to introduce laser light into the waveguide at several different angles which would make it possible to use several transducers of the same center frequency and bandwidth, instead of using transducers of varying center frequencies as is done now. This coupler would also make it trivial to form wide optical illumination apertures. Widening the illumination beam in the guided-wave scanner corresponds optically to increasing the display's numerical aperture. The larger the numerical aperture of the display, the higher the achievable volumetric resolution.

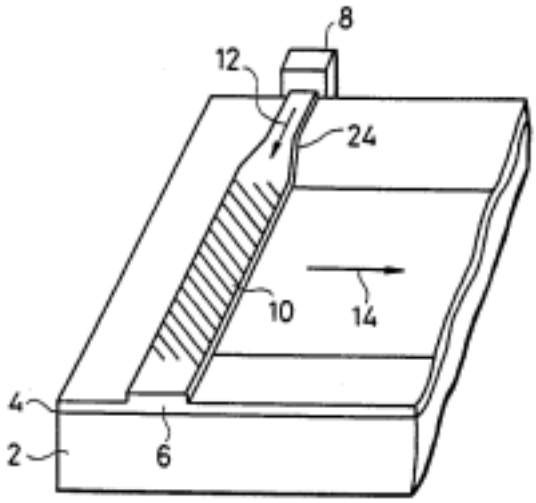

Figure 6-2: This is Figure 12 from US patent number 4,776,661 held by Yuichi Handa.

6.3.2 Improved Confinement

The waveguide scatter should be reduced to as little as possible since it is the only noise created in the operation of the device that cannot be extracted effectively with polarizers. There is the possibility of reducing the scatter in the waveguide by performing an anneal step after proton exchange or by diluting the Benzoic Acid Melt with Lithium Benzoate. Future work could explore these possibilities.

6.3.3 Direct-Write De-Scan HOE

We understand the analytic structure of the HOE so we can generate the pattern computationally and have it written directly by an ebeam writer or an image reduction lab. Quinn Smithwick has already generated computational HOE patterns with good results by simulating the output of our optical HOE recording setup.

6.3.4 Multi-Strip Couplers and other SAW Filter Structures

There are many structures used for the design of SAW components that could be used to enhance the function of the guided-wave scanner. Multi-Strip Couplers can effectively absorb a narrow field of SAW waves and re-radiate a wide field of SAW waves. This type of structure could eliminate the tradeoff between good impedance characteristics and good Bragg diffraction ability in transducer design.

6.3.5 Holovideo on a Chip

The MIT scanned-AOM architecture for holovideo is made of lenses, mirrors and scanning elements. During the past two decades, researchers in the field of integrated optics have been able to fabricate lenses, mirrors and scanning elements as part of waveguide systems on the surface of Lithium Niobate. It is conceivable, therefore, that we could eventually 'pull' all of holovideo's optics, with the possible exception of the output lens, onto an optical chip.

6.4 Concluding Statement

The work reported in this thesis has reached from the description of system-level architecture to the fabrication of nanoscale structures and has provided a foundation for more rapid progress toward the ambitious goal of creating a powerful, mass-producible holographic video display.

Appendix A

Properties of Lithium Niobate

The most commonly used properties of Z-cut Lithium Niobate are included in Table A.1 for the reader's convenience. The values given are approximate and may be reported with some variation in the literature.

Table A.1: Properties of Z-cut Lithium Niobate

Property	Symbol	Value
Extraordinary Index of Refraction	n_e	2.21
Ordinary Index of Refraction	n_o	2.295
PE Extraordinary Index Change	Δn_e	+0.12
PE Ordinary Index Change	Δn_o	-0.05
SAW Velocity, Y Axis	v_y	3909m/s
SAW PE Velocity, X Axis	v_x	3711m/s
SAW Electromechanical Coupling Constant	k^2	.0225
Capacitance per Electrode length	C_g^*	$1.29 * 10^{-9}$F/m

Bibliography

[1] Stephen A Benton. Chapter 6: The diffraction efficiency of gratings. pending publication.

[2] Colin K. Campbell. *Surface Acoustic Wave Devices for Mobile and Wireless Communications*. Academic Press, 1998.

[3] Anna Maria Matteo et. al. Collinear guided wave to leaky wave acoustooptic interactions in proton-exchanged linbo3. *IEEE Transactions on Ultrasonics, Ferroelectrics, and Frequency Control*, 47(1), 1986.

[4] Maurice Stanley et al. 3d electronic holography display system using a 100 megapixel spatial light modulator. In *Proc. of the SPIE*, number 5249, pages 297–308, 2004.

[5] W. Richard Smith et. al. Analysis of interdigital surface wave transducers by use of an equivalent circuit model. *IEEE Transactions on Microwave Theory and Techniques*, MTT-17(11), 1969.

[6] Yuichi Handa. Integrated optical device. US patent number 4,776,661, October 1988.

[7] Stanley Hong. Surface acoustic wave modulators. Master's thesis, MIT, 1988.

[8] Mary Lou Jepsen. Holographic video: Design and implementation of a display system. Master's thesis, MIT, 1989.

[9] V. M. Bove Jr., W. J. Plesniak, T. Quentmeyer, and J. Barabas. Real-time holographic video images with commodity pc hardware. In *Proc. of the SPIE Displays and Applications*, number 5664A, 2004.

[10] Joel S. Kollin. Design and information considerations for holographic television. Master's thesis, MIT, 1988.

[11] Bala Munjuluri Michael L. Huebschman and Harold R. Garner. Dynamic holographic 3-d image projection. *Optics Express*, 11(5):437–445, 2003.

[12] DP Morgan. *Surface-Wave Devices for Signal Processing.* Elsevier, 1991.

[13] Takanori Okoshi. *Three-dimensional Imaging Techniques.* Academic Press, 1976.

[14] Elroy Pearson. Mems devices for holographic video. Master's thesis, MIT, 1988.

[15] Wendy J. Plesniak. *Haptic interaction with Holographic video.* PhD thesis, MIT, 1988.

[16] J[ean-Claude] Poncot. 3ghz bandwidth bragg cells. In *IEEE 1991 Ultrasonics Symposium Proceedings*, volume 1, pages 563–7, 1991.

[17] T. C. Poon, B. W. Schilling, M. H. Wu, K. Shinoda, and Y. Suzuki. Real-time two-dimensional holographic imaging by using an electron-beam-addressed spatial light modulator. *Opt. Lett. 18, 63- (1993).*

[18] Proklov. Multichannel waveguide devices using collinear acoustooptic interaction. *Institute of Radio Engineering and Electronics of the Russian Academy of Sciences*, 1992.

[19] T. J. Hammack R. D. Andrews. title unkown. *J. Polym. Sci. B., 3, 655 (1965)*, 1965.

[20] D. Smalley and Thomas Pastureau. Eigenmode method for fast cascade of p matrices takinging into account mode coupling at reflection. pending release for publication.

[21] M. Solal, V. Laude, and S. Ballandras. A p-matrix based model for saw grating waveguides taking into account modes conversion at the reflection. *IEEE Transactions on Ultrasonics, Ferroelectrics and Frequency Control*, 51(12), 2004.

[22] Pierre St.-Hilaire. *Scalable Architechtures for Holographic Video*. PhD thesis, MIT, 1988.

[23] P.K. Tien and R. Ulrich. Theory of prism-film coupler and thin-film light guides. *Journal of the Optical Society of America*, 60(10), 1970.

[24] Chen Tsai. Guided-wave acousto optic two-dimensional scanner. *Fiber and Integrated Optics*, 1998.

[25] C.S. Tsai. *Guided-Wave Acousto-Optics: Interactions Devices and Applications*. Springer-Verlag, 1981.

[26] J. A. Watlington, M. Lucente, C. J. Sparrell, V. M. Bove Jr., and I. Tamitani. A hardware architecture for rapid generation of electro-holographic fringe patterns. In *Proc. SPIE Practical Holography*, number 2406, 1995.

[27] K.K. Wong. *Properties of Lithium Niobate*. Institution of Engineering and Technology, 2002.